

Microwave absorbing characteristics in Co^{2+} and Al^{3+} substituted $\text{Ba}_{0.5}\text{Sr}_{0.5}\text{Co}_x\text{Al}_x\text{Fe}_{12-2x}\text{O}_{19}$ hexagonal ferrite

Jasbir Singh¹ · Charanjeet Singh^{2,3} · Dalveer Kaur⁴ · S. Bindra Narang³ · Rajshree Jotania⁵ · Rajat Joshi²

Received: 23 June 2016 / Accepted: 3 October 2016 / Published online: 7 October 2016
© Springer Science+Business Media New York 2016

Abstract The Co^{2+} and Al^{3+} ions substituted M-type hexagonal ferrites with chemical composition $\text{Ba}_{0.5}\text{Sr}_{0.5}\text{Co}_x\text{Al}_x\text{Fe}_{12-2x}\text{O}_{19}$ ($x = 0.0, 0.2, 0.4, 0.6, 0.8$ and 1.0) were synthesized by a standard ceramic method. The prepared samples were characterized using X-ray diffraction in order to check phase purity. The absorber testing device method is adopted to investigate microwave absorption of ferrite compositions as a function of frequency, substitution and thickness from 8.2 to 12.4 GHz. The microwave absorption has been evaluated using the standard model of quarter wavelength mechanism and impedance matching mechanism. The microwave absorption is enhanced with the substitution of Co^{2+} and Al^{3+} ions in synthesized Ba–Sr hexagonal ferrites. Composition $x = 1.0$ exhibits good microwave absorber characteristics with 96.94 % absorbed power and -16.4 dB RL at matching frequency and thickness of 11.22 GHz and 2.9 mm respectively.

1 Introduction

The tremendous growth in wireless technology sector has produced electromagnetic pollution attributing to high speed electronic devices operating at micro and millimeter wave regime. This undesired severity renders electromagnetic interference (EMI) leading to the malfunctioning of devices comprising of electrical and electronic circuits. The electronic devices, particularly oscillators or processors operating at GHz, generate harmonics or stray electromagnetic radiation causing bit error in the data received by wireless receivers. Furthermore, when the width of copper tracks of printed circuit boards is near to the quarter wavelength of the passing high frequency GHz signal, these tracks starts working as an antenna and radiate spurious electromagnetic signal referred as EMI. The microwave absorbers or radar absorbing materials (RAM) are used to suppress or attenuate this EMI or stray electromagnetic reflection from military aircraft, tank, radar etc.

Ferrites are employed in communication channel filters, ferrite rod antenna, Faraday law based microwave passive components, radar absorbing materials, tuning slug, radio frequency choke, wideband transformers etc. [1–4]. Their performance in electromagnetic interference (EMI) suppression is better compared to the conventional dielectric counterparts owing to the good magnetic properties. M-type hexagonal ferrites are ferrimagnetic in nature and incorporated particularly as microwave absorber, and exhibit dielectric and magnetic losses, domain wall resonance and ferromagnetic resonance (FMR) associated with spin relaxation [4, 5]. They show high resistivity at microwave frequencies which is pertinent for reducing the unwanted eddy currents.

The various reports are available on the microwave absorption studies in ferrites: Moradi et al. [6] discussed

✉ Charanjeet Singh
charanjeet2003@rediffmail.com

¹ Department of Electronics and Communication Engineering, Yadavindra College of Engineering, Punjabi University, Guru Kashi Campus, Talwandi Sabo, Punjab, India

² Department of Electronics and Communication Engineering, Rayat Bahra Institute of Engineering and Nanotechnology, Hoshiarpur, Punjab, India

³ Department of Electronics Technology, Guru Nanak Dev University, Amritsar, Punjab, India

⁴ Department of Electronics and Communication Engineering, I.K.G. Punjab Technical University, Kapurthla, India

⁵ Department of Physics, Gujarat University, Ahmedabad, Gujarat, India

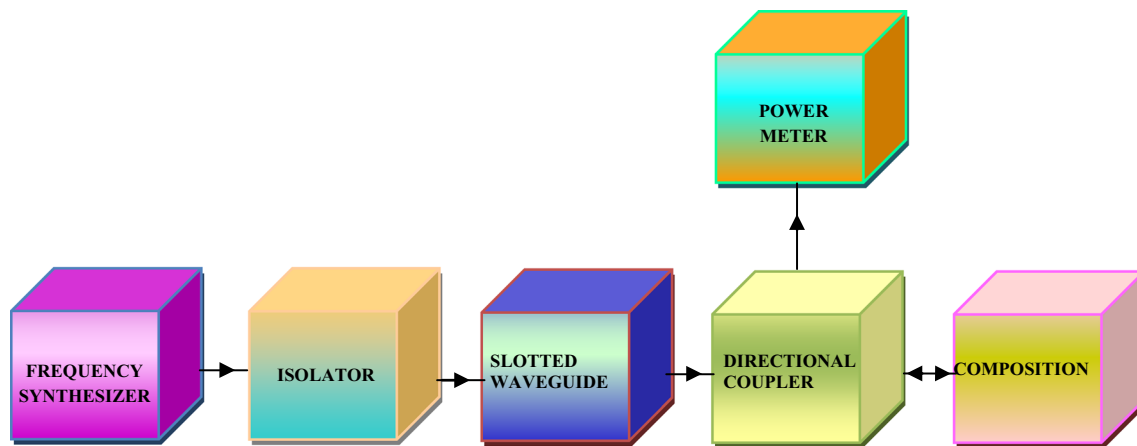


Fig. 1 Block diagram of absorber testing device (ATD) method

the increase in absorption with the thickness of composition and substitution of Mg^{2+} , Mn^{2+} , Co^{2+} and Ti^{4+} ions in M-type Barium ferrite, Moradi et al. [7] also found ~ -14 dB reflection loss around 10 GHz in Zn–Co–Zr substituted M-type $BaFe_{12}O_{19}$ ferrite. Jacobo and Bercoff [8] reported more than 40 dB reflection loss in all compositions of Yt doped Ni–Zn spinel ferrite. Cao et al. [9] reported enhanced absorption with increase in content Mn^{2+} and Ti^{4+} ions in M-type $BaFe_{12-x}(Mn_{0.5}Ti_{0.5})_xO_{19}$ hexagonal ferrite. Sadiq et al. [10] observed increase in absorption with doping of Sm–Mn co-doped X-type hexagonal ferrite around 10.1 GHz. Nam et al. [11] discussed quarter wavelength mechanism and impedance matching mechanism in deciding microwave absorption in La–Sr doped Nickel ferrite. Yu et al. [12] discussed tuning of microwave absorption in Mn–Co doped M-type Barium hexagonal ferrite at Ku-band and obtained observed RL of -30.5 dB in $x = 0.6$ at 2 mm thickness.

In this communication, we report microwave absorption studies in $Ba_{0.5}Sr_{0.5}Co_xAl_xFe_{12-2x}O_{19}$ ($x = 0.0, 0.2, 0.4, 0.6, 0.8$ and 1.0) hexagonal ferrites prepared by a standard ceramic method and elucidated the microwave absorption with the quarter wavelength mechanism and impedance matching mechanism, which to the authors' best knowledge is not reported yet.

2 Experimental

M-type hexagonal ferrite with compositions $Ba_{0.5}Sr_{0.5}Co_xAl_xFe_{12-2x}O_{19}$ ($x = 0.0, 0.2, 0.4, 0.6, 0.8$ and 1.0) were synthesized using a standard ceramic method [13]. In first sintering process; Barium Carbonate (99.9 % pure, Merck), Strontium carbonate (99.98 % pure, Merck), Cobalt carbonate (99.9 % pure, Merck), Aluminium Carbonate (99.9 % pure, Merck) and Ferric Oxide (99.9 % pure, Merck) were chosen as starting materials. The

stoichiometric amount of different chemical reagents of compositions was taken and then grounded well for 8 h with the help of an agate pestle and mortar in the distilled water. The ground mixed powders were pre-sintered at 1000 °C for 10 h in an electric furnace and then slowly cooled to room temperature. In the second sintering process, the obtained powders were re-grounded under the same conditions and pellets of different powder compositions were prepared using a hydraulic press at a uniaxial pressure of 75 KN/m². The prepared pallets were sintered at 1150 °C for 15 h in a furnace and slowly cooled to room temperature. The heating and cooling rate of an electric furnace were set at ± 5 °C/min. The phase purity and M-type crystal structure of compositions were examined using an X-ray diffraction (XRD) technique and XRD patterns of all compositions were recorded at room temperature on X-ray diffractometer—Bruker Model D8, using Cu K α radiation ($\lambda = 1.5405$ Å) in the range of $2\theta = 20^\circ - 70^\circ$.

The microwave characteristics of $Ba_{0.5}Sr_{0.5}Co_xAl_xFe_{12-2x}O_{19}$ ferrites were studied as a function of substitution, frequency and thickness at X-band by absorber testing device (ATD) method [14, 15]: Fig. 1 shows a block diagram of the adopted method.

The microwave frequency synthesizer (HP Model 83751A) generates frequencies from 8.2 to 12.4 GHz in the rectangular slotted waveguide with inner dimensions as length = 22.86 mm, breadth = 10.16 mm. The isolator passes the microwave signal, generated by a synthesizer, in one direction and attenuates in the opposite signal. The directional coupler owes one primary input port and two secondary output ports. The composition, backed by a metal plate, was fitted inside the secondary output port and the reflected microwave signal from the composition was measured by power meter connected to other secondary output port. The power meter Tektronix-Model 3320 was incorporated to measure the microware power of the

reflected microwave signal and S_{11} -parameter was calculated from measured reflected power.

The reflection loss (RL) can be expressed using following equation:

$$RL \text{ (dB)} = 20 \log_{10}(|S_{11}|) \tag{1}$$

The -10 dB reflection loss carries with 90 % microwave absorbed power and the large reflection loss contributes to more microwave absorption and vice versa.

The reflected power (%) was calculated as:

$$\text{Reflected power (\%)} = (P_r/P_{rw}) \times 100 \tag{2}$$

where P_r was the reflected power from the ferrite composition backed by a metal plate and P_{rw} was the reflected power from the metal plate without ferrite composition.

The absorbed power was calculated using the following relation:

$$\text{Absorbed power (\%)} = 100 - \text{reflected power (\%)} \tag{3}$$

The measured or experimental thickness of the ferrite compositions was optimised for maximum microwave absorption: $x = 0.0$ (3.2 mm), $x = 0.2$ (2.8 mm), $x = 0.4$ (2.9 mm), $x = 0.6$ (2.8 mm), $x = 0.8$ (2.9 mm), $x = 1.0$ (3.0 mm). The term matching frequency (f_{mat}) and composition used in manuscript stands for the maximum power absorption at a particular frequency and composition.

3 Results and discussion

3.1 XRD analysis

The structural properties and phase purity of sintered $Ba_{0.5}Sr_{0.5}Co_xAl_xFe_{(12-2x)}O_{19}$ ($x = 0.0, 0.2, 0.4, 0.6, 0.8$ and 1.0) hexaferrite samples were investigated at room temperature using X-ray diffraction technique. Figure 2a–c represents X-ray diffraction patterns of $Ba_{0.5}Sr_{0.5}Co_xAl_xFe_{(12-2x)}O_{19}$ ($x = 0.0-1.0$) hexaferrite samples prepared using a standard ceramic method and sintered at 1150°C for 15 h. All observed peaks in XRD were indexed using Powder-X software with hexagonal magnetoplumbite (M) crystal structure having space group $P6_3/mmc$ (JCPDS file no. 84-0757, $a = 5.892 \text{ \AA}$, $c = 23.183 \text{ \AA}$). JCPDS file no. 19-0098 was used for indexing W-type hexaferrite phase ($BaCo_2Fe_{16}O_{27}$ $a = 5.88 \text{ \AA}$ and $c = 32.84 \text{ \AA}$); while JCPDS file no. 77-2337 was used for indexing orthorhombic spinel crystal structure ($BaFe_2O_4$ $a = 17.34 \text{ \AA}$, $b = 9.335 \text{ \AA}$ and $c = 10.881 \text{ \AA}$).

Lattice parameters ($a = b$ and c) and unit cell volume (V) were calculated using following Eqs. (4) and (5) respectively.

For hexagonal structure $a = b \neq c$ and $\alpha = \beta = 90^\circ$ and $\gamma = 120^\circ$

$$\frac{1}{d_{hkl}^2} = \frac{4}{3} \left(\frac{h^2}{a^2} + \frac{hk}{a^2} + \frac{k^2}{a^2} \right) + \frac{l^2}{c^2} \tag{4}$$

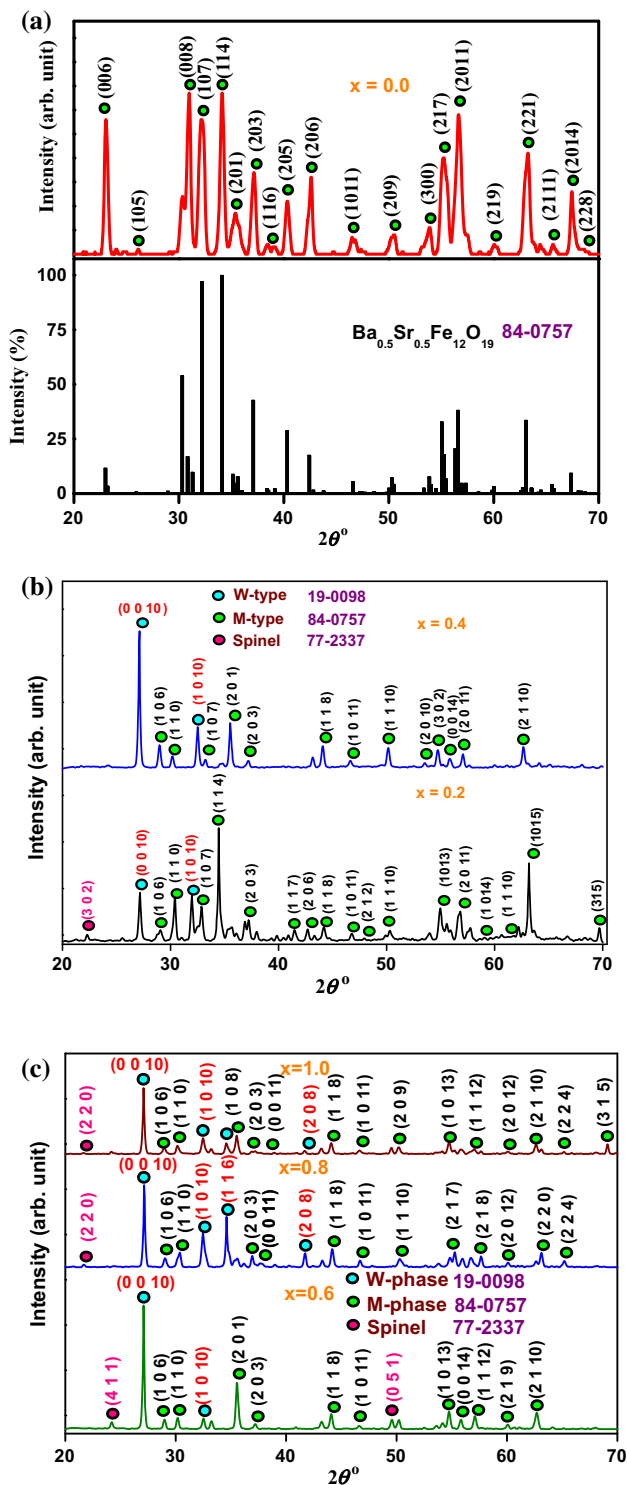
$$\text{Unit cell volume } V = \frac{\sqrt{3}}{2} a^2 c \tag{5}$$

where d_{hkl} is the d-spacing of the lines in XRD pattern and h, k, l are Miller indices.

The lattice parameters, unit cell volume, ratio (c/a), a percentage of phases and crystallite size of all prepared M-type hexaferrite are summarized in Table 1. It is observed that obtained lattice constants (a, c), cell volume (V) values of $Ba_{0.5}Sr_{0.5}Co_xAl_xFe_{(12-2x)}O_{19}$ hexaferrite compositions are slightly lower (except $x = 1.0$, in which lattice constant a value is comparable) than standard values reported in JCPDS file no. 84-0757 of $Ba_{0.5}Sr_{0.5}Fe_{12}O_{19}$ hexaferrite, but well agreed for W and S phases. The crystallite size of formed hexaferrite powders was found in the range between 51 and 68 nm (error $\pm 5\%$). The XRD analysis of $x = 0.0$ composition confirms the formation of single M-type phase (hexagonal); and $x = 0.2-1.0$ compositions show mixed crystalline phases of M (hexagonal), W (hexagonal) and $BaFe_2O_4$ (spinel) but all compositions show magnetoplumbite phase as a major phase. The high intense W-phase peaks are observed in XRD patterns of compositions $x = 0.4-1.0$ (Fig. 2); while compositions $x = 0.0$ and 0.2 possess high intense XRD peaks of M-phase only. It seems M phase gets merged with W phase in $x = 0.4-1.0$ compositions, hence, the peak intensity of W peaks is high. It was reported by Smith and Wijn [16] that the unit cell of M-type phase is very closely related with W-type phase; the only difference in successive R blocks; which are interplaced between one S-block instead of two S- blocks as in W-type phase. It can be also observed from Table 1 that there is slight an increase in lattice parameters and unit cell volume values after doping of Co–Al in prepared hexaferrite compositions except in composition $x = 0.0$, which is closed to standard JCPDS values. It is attributed to ionic radii of Co^{2+} (0.72 \AA), Al^{3+} (0.51 \AA), and Fe^{2+} (0.64 \AA) [17, 18]. It seems that Co–Al substitution in the prepared hexagonal ferrite has disturbed crystal symmetry and this fact confirms from (c/a) ratio which is slight increased, indicating a change in the crystal structure by the doping of Co–Al ions in prepared barium strontium hexaferrite compositions.

3.2 Reflection loss, microwave absorbed power

Figure 3 displays the variation of reflection loss (RL) as a function of frequency and substitution of Co^{2+} and Al^{3+} ions in $Ba_{0.5}Sr_{0.5}Co_xAl_xFe_{12-2x}O_{19}$ ferrite. The reflection loss increases with the substitution of Co^{2+} and Al^{3+} ions and all compositions exhibit RL more than -10 dB at low,



middle and high frequency regime; compositions display highest RL (> -14 dB) at 11.22 GHz. The substitution of Co^{2+} and Al^{3+} ions renders (1) change in amplitude of RL peaks, (2) nearly no shift of peaks along the entire frequency region accompanied by the same peaks of maximal and minimal values almost at the same frequencies;

Fig. 2 a The XRD patterns of $\text{Ba}_{0.5}\text{Sr}_{0.5}\text{Co}_x\text{Al}_x\text{Fe}_{(12-2x)}\text{O}_{19}$ ($x = 0.0$) hexaferrite compositions, prepared using double sintering ceramic method and sintered at 1150°C for 15 h and standard JCPDS pattern of M-type $\text{Ba}_{0.5}\text{Sr}_{0.5}\text{Fe}_{12}\text{O}_{19}$ (file no. 84-0757) hexagonal ferrite. **b** The XRD patterns of $\text{Ba}_{0.5}\text{Sr}_{0.5}\text{Co}_x\text{Al}_x\text{Fe}_{(12-2x)}\text{O}_{19}$ ($x = 0.2$ and 0.4) hexaferrite compositions, prepared using a standard ceramic method and sintered at 1150°C for 15 h. **c** The XRD patterns of $\text{Ba}_{0.5}\text{Sr}_{0.5}\text{Co}_x\text{Al}_x\text{Fe}_{(12-2x)}\text{O}_{19}$ ($x = 0.6, 0.8$ and 1.0) hexaferrite compositions, prepared using a standard ceramic method and sintered at 1150°C for 15 h

$x = 1.0$ maintains large RL of -16.4 dB among all the compositions.

Figure 4 displays the variation of absorbed power (P_{ab}) as a function of frequency and substitution of Co^{2+} and Al^{3+} ions. The large P_{ab} is observed at higher substitution along the investigated frequency region and more dispersion is seen from 9.04 to 10.38 GHz. The absorbed power is more than 90 % in all compositions along the different frequency regions. Composition $x = 1.0$ and 0.2 show highest and lowest P_{ab} of 97.7 and 19.2 % at 11.22 and 11.89 GHz respectively; $x = 1.0$ has large P_{ab} among all compositions at number of investigated frequencies.

Table 2 shows maximum absorbed (P_{amax}) with corresponding matching frequency (f_{mat}) in $\text{Ba}_{0.5}\text{Sr}_{0.5}\text{Co}_x\text{Al}_x\text{Fe}_{12-2x}\text{O}_{19}$ ferrite; P_{amax} increases with the substitution of Co^{2+} and Al^{3+} ions. All compositions have P_{amax} at the same f_{mat} of 11.22 GHz; $x = 1.0$ has highest P_{amax} of 97.7 %.

3.3 Quarter wavelength mechanism

According to this mechanism [19, 20] when the thickness of ferrite absorber is equal to the $1/4$ th wavelength of the microwave signal, it will get attenuated or absorbed after passing through ferrite material.

When the microwave signal propagates through the ferrite composition backed by a metal plate, a part of it will be partially reflected by the front surface of ferrite and the remaining signal will be transmitted through the ferrite. This transmitted signal gets reflected after reaching the metal plate and arrives again at the front face of the ferrite. When the reflected signal from the front surface of ferrite composition is equal in magnitude and 180° out of phase with the reflected signal from the metal plate, both signals will cancel each other and total reflection will be zero. Therefore, this condition can be mathematically expressed as:

$$t_m = \frac{n\lambda_0}{4\sqrt{\mu\epsilon}} \quad n = 1, 3, 5, \dots \quad (6)$$

where t_m , λ_0 , ϵ , and μ denote matching thickness, wavelength, complex permittivity, complex permeability and

Table 1 Bragg angle and FWHM (high intense peak) lattice parameters, cell volume, ratio (*c/a*), percentage of phases of Ba_{0.5}Sr_{0.5}Co_xAl_xFe_(12–2x)O₁₉ (*x* = 0.0, 0.2, 0.4, 0.6, 0.8 and 1.0) hexaferrite

compositions, prepared using a standard ceramic method and sintered at 1150 °C for 15 h

| Co–Al content (<i>x</i>) | 2θ (°) | FWHM | Lattice constants | | Ratio <i>c/a</i> | Unit cell volume (<i>V</i>) (Å ³) | Percentage of phases | | |
|----------------------------|--------|--------|-------------------------|--------------|------------------|---|----------------------|-------|-------|
| | | | <i>a</i> = <i>b</i> (Å) | <i>c</i> (Å) | | | M (%) | W (%) | S (%) |
| 0.0 | 34.211 | 0.1217 | 5.886 | 23.136 | 3.931 | 694.139 | 100 | 0 | 0 |
| 0.2 | 34.461 | 0.1373 | 5.867 | 23.038 | 3.926 | 686.744 | 85 | 10 | 5 |
| 0.4 | 27.116 | 0.1534 | 5.868 | 23.058 | 3.929 | 687.575 | 85.71 | 14.29 | 0 |
| 0.6 | 27.090 | 0.1327 | 5.872 | 23.062 | 3.927 | 688.632 | 73.34 | 13.33 | 13.33 |
| 0.8 | 27.146 | 0.1533 | 5.879 | 23.125 | 3.933 | 692.160 | 70.59 | 23.53 | 5.88 |
| 1.0 | 27.088 | 0.1584 | 5.899 | 23.145 | 3.924 | 697.480 | 73.69 | 21.05 | 5.26 |

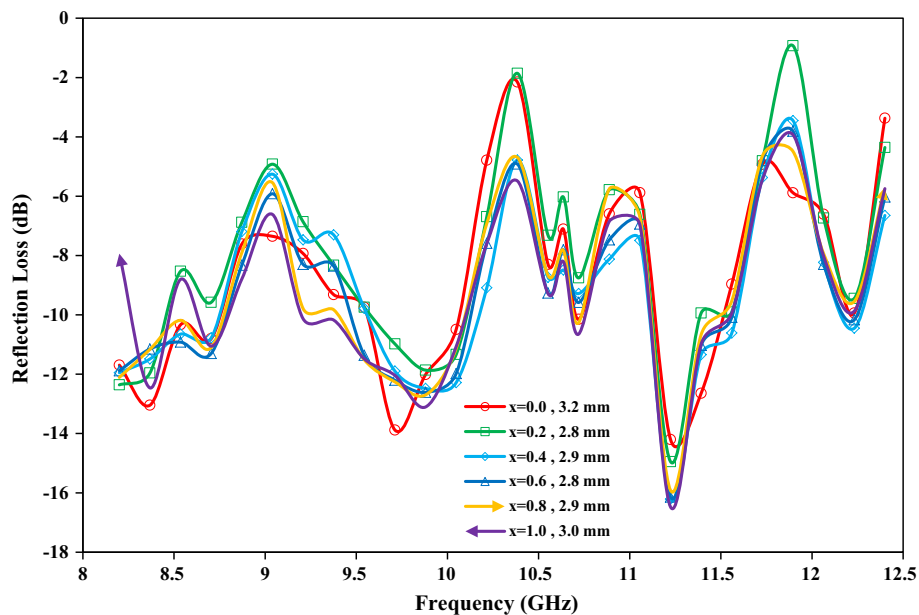


Fig. 3 Plots of reflection loss versus frequency and substitution in Ba_{0.5}Sr_{0.5}Co_xAl_xFe_{12–2x}O₁₉ferrites (*x* = 0.0, 0.2, 0.4, 0.6, 0.8 and 1.0)

velocity of light respectively; Nicholson–Ross method [21] is used to derive ϵ and μ from S-parameters.

Table 2 depicts various parameters related to the quarter wavelength mechanism applied in different compositions. For observed RL peak or maximum absorption (Figs. 3, 4) at 11.22 GHz, composition *x* = 0.2, 0.6 and 0.8 govern the quarter wavelength mechanism; the measured or experimental thickness of compositions is approximately equal to the theoretical thickness calculated using Eq. (6) of this mechanism ($t = \lambda_o/4$). However, this mechanism is not satisfied in *x* = 0.4 accompanied by the difference in experimental and calculated thickness.

Table 1 implies that *x* = 1.0 constitutes all RL peaks of more than –10 dB. It also shows –10 dB bandwidth displayed by the compositions; –10 dB bandwidth means the band of frequencies for which RL is >–10 dB. Composition *x* = 0.8 and 1.0 infer 840 MHz absorption bandwidth

(ABW) at the same frequency band from 9.37 to 10.21 GHz, while *x* = 0.0 and 0.2 have ABW of 500 and 670 MHz from 9.54 to 10.04 and 9.54–10.21 GHz respectively.

3.4 Impedance matching mechanism

The input impedance (Z_{in}) of a single layer absorber can be calculated theoretically on the basis of transmission line theory as [22]:

$$Z_{in} = Z_o(\mu/\epsilon)^{1/2} \tanh \left[j(2\pi ft/c) (\mu \epsilon)^{1/2} \right] \tag{7}$$

where $Z_o = 377 \Omega$ is the characteristic impedance of free space and *t*, *f*, ϵ , μ , *c* denote thickness, frequency, complex permittivity, complex permeability and velocity of light respectively.

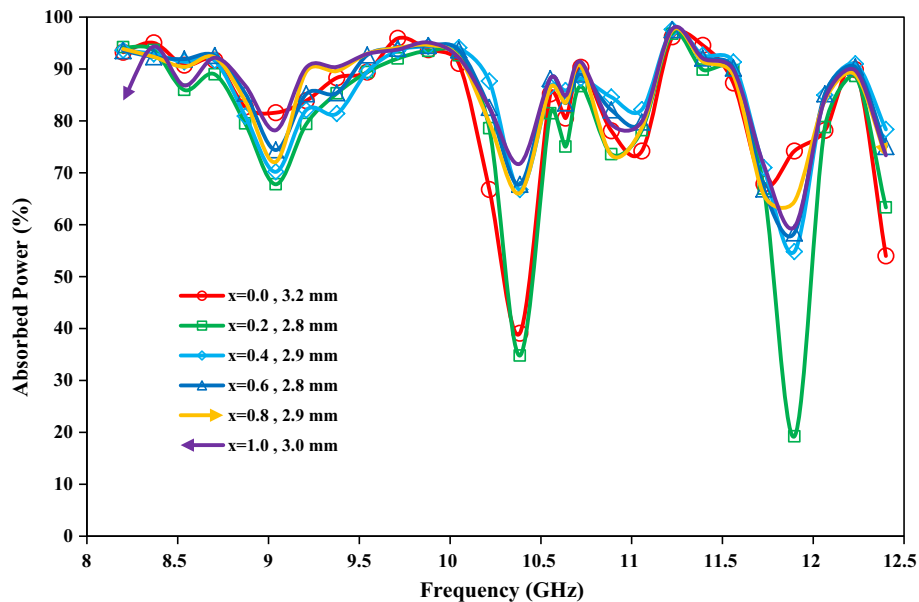


Fig. 4 Plots of absorbed power versus frequency and substitution in $\text{Ba}_{0.5}\text{Sr}_{0.5}\text{Co}_x\text{Al}_x\text{Fe}_{12-2x}\text{O}_{19}$ ferrites ($x = 0.0, 0.2, 0.4, 0.6, 0.8$ and 1.0)

Table 2 Maximum absorbed power, matching frequency, calculated thickness, matching thickness, frequency band and bandwidth for $\text{RL} > -10$ dB in $\text{Ba}_{0.5}\text{Sr}_{0.5}\text{Co}_x\text{Al}_x\text{Fe}_{12-2x}\text{O}_{19}$ ferrites

| Composition | P_{amax} (%) | Matching frequency (f_{mat}) (GHz) | Thickness $t = \lambda/4$ (mm) (calculated) | Matching thickness (mm) (measured) | Frequency band $\text{RL} > -10$ dB (GHz) | Bandwidth (MHz) |
|-------------|-----------------------|---|---|------------------------------------|---|-----------------|
| $x = 0.0$ | 96.2 | 11.22 | 3.0 | 3.2 | 9.54–10.04 | 500 |
| $x = 0.2$ | 96.8 | 11.22 | 2.9 | 2.8 | 9.54–10.21 | 670 |
| $x = 0.4$ | 97.6 | 11.22 | 2.2 | 2.9 | – | – |
| $x = 0.6$ | 97.5 | 11.22 | 2.7 | 2.8 | – | – |
| $x = 0.8$ | 97.4 | 11.22 | 3.0 | 2.9 | 9.37–10.21 | 840 |
| $x = 1.0$ | 97.7 | 11.22 | 3.1 | 3.0 | 9.37–10.21 | 840 |

When Z_{in} is equal to Z_o , input impedance of composition will be equal to characteristic impedance contributing infinite absorption of the signal by the composition.

The Eq. 7 explains that Z_{in} is of complex form ($a + j b$) where a is the real part and b is the imaginary part: (1) Theoretically, all signal will be absorbed if $|Z| = Z_o = 377\Omega$, i.e. $Z_{\text{real}} = 377\Omega$ and $Z_{\text{img}} = 0$, (2) a component of signal RL will be absorbed when $Z_{\text{real}} \neq 377\Omega$ and/or $Z_{\text{img}} \neq 0$; when Z_{in} is equal or near to Z_o (377Ω), it attributes to large microwave absorption due to impedance matching. Furthermore, absorption decreases when Z_{real} moves farther from 377Ω and/or Z_{img} increases (positive or negative values).

Table 3 summarizes Z_{in} , Z_{real} and Z_{img} values corresponding to the large microwave absorption or RL peaks observed in compositions. Composition $x = 0.4$ has relatively both Z_{real} and Z_{img} more close to 377Ω and zero

than other compositions, thereby giving RL peaks at different frequencies due to the impedance matching mechanism. The other compositions have either Z_{real} away from 377Ω or Z_{img} away from zero and thus impedance matching mechanism is not satisfied; for example $x = 0.0$ owe $Z_{\text{real}} = 377.8\Omega$ which is nearly equal to $Z_o = 377\Omega$, however, $Z_{\text{img}} = -271.5\Omega$ makes far away from $Z_{\text{img}} = 0$. Similar variation was reported by Nam et al. [11] in $\text{La}_{1.5}\text{Sr}_{0.5}\text{NiO}_4$ ferrites.

3.5 Screenshot of microwave signal

The screenshots show the frequency, phase and amplitude of the signal while passing through different compositions. Figure 5 displays the observation of input signal applied to the compositions and signal transmitted from the compositions, and cathode ray oscilloscope (CRO) is used to

Table 3 Impedance matching mechanism with f , Z_{in} , Z_{real} and Z_{img} values corresponding to RL peaks in $Ba_{0.5}Sr_{0.5}Co_xAl_xFe_{12-2x}O_{19}$ ferrites

| f (GHz) | RL peak (dB) | Z_{in} (Ω) | Z_{real} (Ω) | Z_{img} (Ω) | RL peak (dB) | Z_{in} (Ω) | Z_{real} (Ω) | Z_{img} (Ω) | RL peak (dB) | Z_{in} (Ω) | Z_{real} (Ω) | Z_{img} (Ω) |
|----------------|--------------|-----------------------|-------------------------|------------------------|--------------|-----------------------|-------------------------|------------------------|--------------|-----------------------|-------------------------|------------------------|
| <i>x = 0.0</i> | | | | | | <i>x = 0.2</i> | | | | | | |
| 8.36 | -13.0 | 552.1 | 528.4 | -160.2 | -11.9 | 91.1 | 51.7 | -75.1 | -11.4 | 92.6 | 92.3 | 8.2 |
| 8.70 | -10.8 | 465.2 | 377.8 | -271.5 | -9.5 | 92.3 | 61.7 | -68.6 | -10.7 | 89.2 | 89.1 | 4.1 |
| 9.20 | -7.9 | 332.0 | 227.5 | -241.8 | -6.8 | 80.0 | 46.3 | -65.2 | -7.4 | 86.6 | 86.5 | 4.2 |
| 9.71 | -13.8 | 261.9 | 156.9 | -209.7 | -10.9 | 58.6 | 35.9 | -46.3 | -11.8 | 83.7 | 83.5 | 5.7 |
| 9.88 | -12.0 | 243.1 | 138.0 | -200.1 | -11.8 | 52.5 | 37.4 | -36.8 | -12.4 | 84.7 | 84.3 | 7.8 |
| 10.72 | -10.1 | 159.9 | 78.5 | -139.2 | -8.7 | 47.2 | 43.9 | -17.3 | -9.2 | 87.7 | 87.5 | 5.3 |
| 11.22 | -14.2 | 126.4 | 64.8 | -108.5 | -14.9 | 58.9 | 55.4 | -20.0 | -16.2 | 87.8 | 87.7 | 3.5 |
| 12.23 | -9.9 | 81.0 | 47.4 | -65.8 | -9.4 | 39.2 | 38.6 | -6.8 | -10.4 | 81.8 | 81.8 | 1.3 |
| <i>x = 0.6</i> | | | | | | <i>x = 0.8</i> | | | | | | |
| 8.36 | -11.1 | 109.2 | 103.4 | -35.1 | -11.1 | 113.8 | 100.5 | -53.3 | -12.4 | 175.9 | 123.7 | -125.0 |
| 8.70 | -11.3 | 108.3 | 102.3 | -35.5 | -11.1 | 111.3 | 98.8 | -51.3 | -11.0 | 163.2 | 114.7 | -116.1 |
| 9.20 | -8.2 | 105.3 | 99.0 | -35.9 | -9.7 | 107.0 | 95.3 | -48.6 | -10.1 | 145.7 | 103.4 | -102.6 |
| 9.71 | -12.2 | 98.9 | 92.8 | -34.2 | -12.2 | 98.4 | 87.7 | -44.5 | -12.0 | 129.6 | 92.0 | -91.3 |
| 9.88 | -12.6 | 97.5 | 92.3 | -31.4 | -12.7 | 95.7 | 86.8 | -40.2 | -13.1 | 123.3 | 89.8 | -84.5 |
| 10.72 | -9.5 | 95.9 | 91.0 | -30.3 | -10.2 | 95.1 | 88.2 | -35.6 | -10.6 | 113.7 | 89.8 | -69.7 |
| 11.22 | -16.1 | 93.4 | 89.0 | -28.2 | -15.9 | 91.9 | 85.9 | -32.8 | -16.4 | 108.7 | 87.8 | -64.0 |
| 12.23 | -10.1 | 87.9 | 83.0 | -28.8 | -9.5 | 85.9 | 80.2 | -30.7 | -9.8 | 99.4 | 81.4 | -57.0 |

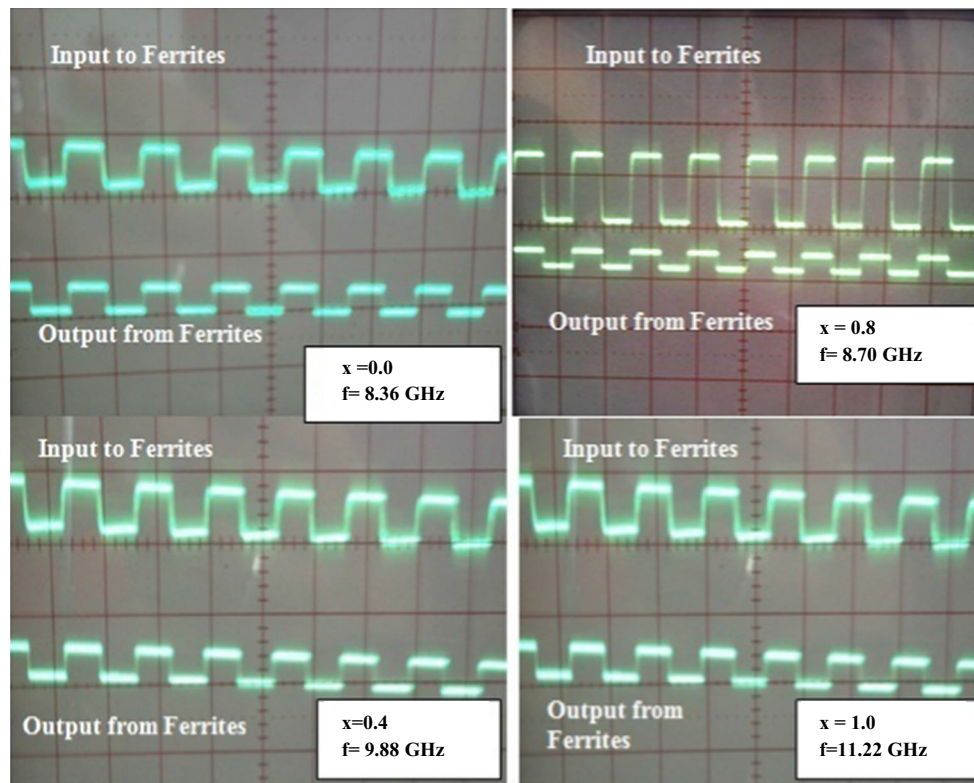


Fig. 5 Screenshots of the input signal and signal transmitted through the ferrite compositions (amplitude value of the signal is a guide to the eye)

display these signals: different frequencies applied to composition $x = 0.0, 0.4, 0.8$ and 1.0 are 8.36, 9.88, 8.70 and 11.22 GHz respectively. These screenshots depict the only attenuation in the signal by compositions and frequency as well as phase of signal remain unchanged. Similar variation was also noted for other applied frequencies and $x = 0.2$ as well as $x = 0.6$ also exhibit the same behavior.

4 Conclusions

1. The microwave absorption increases with substitution of Co^{2+} and Al^{3+} ions in prepared $\text{Ba}_{0.5}\text{Sr}_{0.5}\text{Co}_x\text{Al}_x\text{Fe}_{12-2x}\text{O}_{19}$ ferrite.
2. The quarter wavelength and impedance matching mechanism can be implemented to decide thickness and frequency for maximum microwave absorption and design microwave absorbers.
3. Composition $x = 0.0, 0.2, 0.6, 0.8$ and 1.0 have contribution of quarter wavelength mechanism for large microwave absorption. Composition $x = 0.4$ confirms the impedance matching mechanism for observed microwave absorption.
4. Composition $x = 1.0$ exhibits microwave absorber or EMI reduction characteristics with 97.7 % absorbed power at matching frequency and thickness of 11.22 GHz and 3.0 mm respectively.
5. Composition $x = 0.8$ and 1.0 have -10 dB absorption bandwidth of 840 MHz while $x = 0.0$ and 0.2 owe 500 and 670 MHz respectively.
6. The prepared compositions depict potential for different electromagnetic or microwave absorber applications by proper tuning of frequency, substitution and thickness in their compositions, which is a topic of separate investigation.

References

1. J.C. Apesteguy, A. Pamiani, D. Digiovanni, S.E. Jacobo, *Phys. B* **404**, 2713 (2009)
2. X. Huang, J. Zhang, M. Lai, T. Sang, *J. Alloys Compd.* **627**, 67 (2015)
3. U.R. Lima, M.C. Nasar, M.C. Rezende, J.H. Araugo, *J. Magn. Magn. Mater.* **320**, 1666 (2008)
4. P. Meng, K. Xiong, L. Wang, S. Li, Y. Cheng, G. Xu, *J. Alloys Compd.* **628**, 75 (2015)
5. J. Liu, J. Zhang, P. Zhang, S. Wang, C. Lu, Y. Li, M. Zhang, *Mater. Lett.* **158**, 53 (2015)
6. R.S. Alam, M. Moradi, H. Nikmanesh, J. Ventura, M. Rostami, *J. Magn. Magn. Mater.* **402**, 20 (2016)
7. R.S. Alam, M. Moradi, M. Rostami, H. Nikmanesh, R. Moayedi, Y. Bai, *J. Magn. Magn. Mater.* **381**, 1 (2015)
8. S.E. Jacobo, P.G. Bercoff, *Ceram. Int.* **42**, 7664 (2016)
9. K.-K. Ji, Y. Li, M.-S. Cao, *J. Mater. Sci. Mater. Electron.* **27**, 5128 (2016)
10. I. Sadiq, S. Naseem, M.N. Ashiq, M.A. Iqbal, I. Ali, M.A. Khan, S. Niaz, M.U. Rana, *J. Magn. Magn. Mater.* **406**, 184 (2016)
11. P.T. Tho, C.T.A. Xuan, D.M. Quang, T.N. Bach, T.D. Thanh, N.T.H. Le, D.H. Manh, N.X. Phuc, D.N.H. Nam, *Mater. Sci. Eng. B* **186**, 101 (2014)
12. L. Wang, H. Yu, X. Ren, G. Xu, *J. Alloys Compd.* **588**, 212 (2014)
13. C. Singh, S. Bindra Narang, I.S. Hudiara, Y. Bai, *J. Alloys Compd.* **464**, 429 (2008)
14. M.R. Meshram, N.K. Agrawal, B. Sinha, P.S. Misra, *J. Magn. Magn. Mater.* **271**, 2007–2014 (2004)
15. P. Singh, V.K. Babbar, A. Razdan, R.K. Puri, T.C. Goel, *J. Appl. Phys.* **87**, 4362 (2000)
16. J. Smit, H.P.J. Wijn, *Ferrites* (Philips Technical Library, Wiley, New York, 1959)
17. C. Singh, S. Bindra Narang, I.S. Hudiara, Y. Bai, F. Tabatabaei, *Mater. Res. Bull.* **43**, 176 (2008)
18. D.R. Mane, U.N. Devatwal, K.M. Jadhav, *Mater. Lett.* **44**, 91 (2000)
19. B. Wang, J. Wei, Y. Yang, T. Wang, F. Li, *J. Magn. Magn. Mater.* **323**, 1101 (2011)
20. N.-N. Song, Y.J. Ke, H.-T. Yang, H. Zhang, X.-Q. Zhang, B.-G. Shen, Z.-H. Cheng, *Sci. Rep.* **2291**, 1 (2013)
21. A.M. Nicolson, G.F. Ross, *IEEE Trans. Instrum. Meas.* **19**, 377 (1970)
22. T. Inui, K. Konishi, K. Oda, *IEEE Trans. Magn.* **35**, 3148 (1999)